Enhancement of hidden structures of early skin fibrosis using polarization degree patterns and Pearson correlation analysis

Alexander P. Sviridov
National Institutes of Health
Bethesda, Maryland 20892
    and
Institute for Laser and Information Technologies
    of Russian Academy of Sciences
Troitsk, Moscow Region, 142190
Russia

Victor Chernomordik
Moinuddin Hassan
National Institutes of Health
Bethesda, Maryland 20892
E-mail: vchern@helix.nih.gov

Albert C. Boccara
Ecole Superinieure de Physique et de Chimie
    Industrielle de Paris (ESPCI)
10 Rue Vauquelin, Paris 75005
France

Angelo Russo
Paul Smith
Amir Gandjbakhche
National Institutes of Health
Bethesda, Maryland 20892

Abstract. The skin of athymic nude mice is irradiated with a single dose of x-ray irradiation that initiated fibrosis. Digital photographs of the irradiated mice are taken by illuminating the mouse skin with linearly polarized probe light of 650 nm. The specific pattern of the surface distribution of the degree of polarization enables the detection of initial skin fibrosis structures that were not visually apparent. Data processing of the raw spatial distributions of the degree of polarization based on Fourier filtering of the high-frequency noise improves subjective perception of the revealed structure in the images. In addition, Pearson correlation analysis provides information about skin structural size and directionality. © *2005 Society of Photo-Optical Instrumentation Engineers.* [DOI: 10.1117/1.2073727]

1 Introduction

Mapping the degree of polarization (DP) of backscattered light with respect to its initial polarization can provide valuable diagnostic information about the superficial and subsurface structures of the skin. It can be used to extract tissue characteristics that are impossible to discern from conventional visual or photographic methods. One of the major strengths of polarization measurements is the ability to separate the light backscattered from superficial tissue layers and the multiple scattered lights coming from much deeper tissue layer.[1] This distinction is based on conservation of initial polarization state in the superficial tissue layer while in the deeper tissue the light becomes depolarized. For this reason, polarization analysis can be used to extract tissue characteristics that conventional visual or photographic methods are not capable of discerning.[2–5] Recent technological advances have resulted in the design of a handheld polarized light camera that may further expand medical applications of the polarization degree mapping.[6] Several optical characteristics of the tissue determine changes in polarization state of the backscattered light relative to the incident light. First, the polarization state of the incident beam can be modified by the specular reflection from the surface heterogeneities. Second, the spatial variations of the light absorption coefficient influence the mean path of the detected photons inside the tissue. Higher absorption coefficients result in smaller average pathlengths of detected photons and, therefore, a higher polarization degree of light, backscattered from the regions with increased absorption[7] (to make this effect visible, one should exclude multiply scattered photons from detection, because scattering quickly randomizes the polarization state of photons). And third, the tissue may have an anisotropic birefringence effect due to structural anisotropy. For example, rods or fibers could change the degree of polarization according to the mutual orientation of their axes and polarization vectors.[8]

Analysis of the 2-D distributions of DP can help to reveal such anisotropic structural features. For example, to evaluate the presence and extent of skin fibrosis developing after an injury (initiated either by burns, trauma, or ionizing radiation used to treat cancer), polarization images can be investigated. The skin dermis can be characterized by the density and preferential orientation of collagen fibers. As a result of an incurred injury, collagen fibers within the dermis may organize into bundles that are not observed as structural components of

Address all correspondence to Victor Chernomordik, NICHD, National Inst. of Health, Bldg 9, Rm B1E11, Bethesda, MD 20892. Tel.: (301) 435-9236; Fax: (301) 435-9236; E-mail: vchern@helix.nih.gov
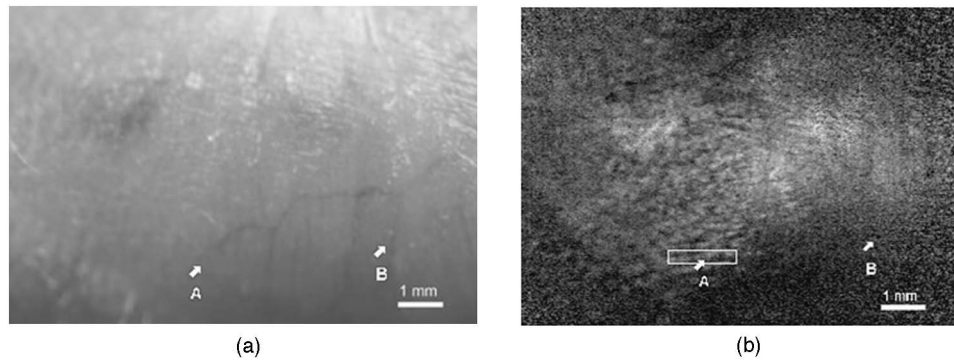
Fig. 1 (a) Gray-scale visual image of the nude mouse skin 20 days after x-ray irradiation and (b) the image of the DP in 8-bit gray-scale format that corresponds to the same area as in (a), where points *A* and *B* represent x-ray irradiated and nonirradiated areas, respectively.

the normal skin.[9,10] The ability to determine the structural components of skin with incipient fibrosis may enable physicians to avoid keloid formation and radiation treatment overdoses, or intervene with an antifibrotic treatment at an earlier stage.[11–14] Unfortunately, due to the highly scattering nature of tissue, in many cases, the relationship between the observed polarization of detected light and internal skin structure is distorted by depolarization, resulting from multiple scattering of photons. Surface roughness as well as speckle may also blur the image. For example, in the case of optical coherent tomography Rogowska and Brezinski observed image distortion due to speckles.[15] Additional distortions of noisy polarization degree images can be easily introduced by data processing. Therefore, it is important to develop special procedures to enhance the internal skin structures, such as fibrosis, from noisy digital images. This paper demonstrates the effectiveness of polarized digital photography for visualization of skin fibrosis structures. The algorithm, based on Pearson correlation analysis, was developed for the polarization imaging of the tissue surface, and characterization of the size and orientation of heterogeneities within the skin fibrosis zone.

2 Materials and Methods

The protocol used in this study was institutionally approved in accordance with the guidelines of the Institute of Laboratory Animal Resources, National Research Council. For this study, athymic nude mice were immobilized and a selected area of skin on the right flank was irradiated with an x-ray irradiation dose of 30 Gy. The area of treatment was approximately 20 $\times$ 20 mm^2. Such treatment typically causes earlier fibrosis of the dermal layer of the skin,[10,16] which developed during 2 to 3 weeks after irradiation. The measurements of polarization degree were performed 20 days after x-ray exposure.

The mouse skin was illuminated by an expanded linearly polarized probe light from a diode laser of 650 nm wavelength. A digital camera (EOS D60, Canon Inc. Japan) with an objective of 0.31 m focal length was used to produce images of the mouse skin. The images were recorded into files that showed the intensity distribution of the detected red light. Each image was 3072×2048 pixels and the output of each pixel consisted of a 16-bit digital signal. The distance between the neighboring pixels corresponded to a physical distance of

approximately 0.0075 mm on the surface of the object. Calibration of the camera response for wide beams was performed using a set of neutral density filters. The camera response was linear in the range of light intensities used in the experiments. The probe beam was aimed at an angle of approximately 15 deg relative to the direction of normal to the mouse skin surface, while the camera objective axis was parallel to this normal. Such orientation prevented a specularly reflected probe beam from reaching the objective. A polarization analyzer was positioned in front of the camera objective. The transmission axis was either parallel or perpendicular to the polarization vector of the incident beam, providing copolarized or cross-polarized images, respectively. The light of the diode laser backscattered from mouse skin created speckles in the front of the camera matrix. The speckle was estimated to be 1 to 2 pixels, while the appropriate intensity variance was 5 to 10%. This enabled us to ignore the influence of the speckles on the recorded image.

3 Fast Fourier Transform Filtering

A conventional visual image of the x-ray-irradiated zone 20 days after radiation is shown in Fig. 1(a). No feature changes of the skin structure can be observed.

The matrix of the degree of polarization of the backscattered light with respect to its initial polarization can be shown as[1]

$$\mathbf{G} = \frac{\mathbf{I}_{par} - \mathbf{I}_{per}}{\mathbf{I}_{par} + \mathbf{I}_{per}}, \qquad (1)$$

where $\mathbf{I}_{par}$ and $\mathbf{I}_{per}$ are matrices of copolarized and cross-polarized images, respectively. Note that Eq. (1) is not a rigorous definition of the degree of polarization. Strictly speaking, the degree of polarization should be determined from the Stokes vector or equivalents approach.[17] Then it can be used to take into account variations in circular polarization that are neglected in Eq. (1), or rotation of the polarization vector of the whole beam due to reflections etc. However, in our case of media, i.e., tissue, birefringence effects are weak (optical anisotropy of the mouse skin is expected to be negligible), and do not result in a noticeable rotation of the polarization vector of initially linearly polarized beam or creation of circularly polarized components in the backscattered light.[18] Therefore,
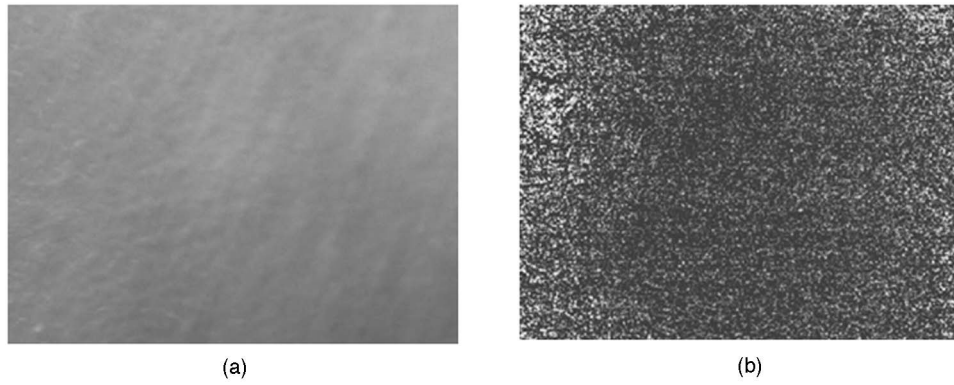
Fig. 2 (a) Conventional visual image of untreated area of a mouse and (b) the corresponding image of the DP.

matrix **G** is a good approximation to the spatial distribution of the genuine polarization degree of the backscattered probe light. We can also neglect fine effects, predicted for propagation of partially coherent polarized light in free space.[19] These effects can, in principle, result in some variations of the polarization state of radiation, but these distortions are observable only for very special experimental conditions, e.g., anisotropy in the spatial degree of correlation of different components of the electric vector in the source plane and large distances of propagation (>1 to 10 m). In our case, the distance between the source and detector is too small to produce any significant changes of polarization state on propagation. Besides, our optical system does not change the polarization state of radiation because it produces an image of the object in the detector plane.

The image of matrix **G**, corresponding to the conventional visual image of Fig. 1(a), is presented in Fig. 1(b), where the irradiated zone in the central part of the field marked A can be distinguished from the background zones of the periphery marked B. Similar patterns were also observed in the x-ray-irradiated area of additional mice 20 days after irradiation. A typical image of nonirradiated mouse skin [see Fig. 2(a)] revealed no actual difference throughout the pattern of the degree of polarization as shown in Fig. 2(b). The observed difference in Fig. 1(b) may be attributed to the presence of collagen bundles observed in histological patterns.[9] These bundles are formed in the dermis as a result of x-ray irradiation. Despite visualizing some features, the polarization degree pattern is significantly distorted by high-spatial-frequency noise. The **G** matrix is formed from the raw data in the space domain. It has been transformed into a spatial frequency domain matrix **G**′ by discrete fast Fourier transform (FFT). This transform has been realized by the *cfft* function of Mathcad 12, applicable to matrices of an arbitrary size. Particular spatial frequencies were filtered out from the signal by replacing corresponding elements of matrix **G**′ with zeroes:

$$G''_{i,j} = \begin{cases} 0, & \text{if } (i < k) \text{ AND } (j < k) \\ 0, & \text{if } (i > K) \text{ OR } (j > K) \\ G'_{i,j}, & \text{otherwise,} \end{cases} \quad (2)$$

where i and j are indices of the matrix elements; k and K are low and high limiting indices, respectively, characterizing the

applied spatial frequency filter. A new space domain matrix, corresponding to the modified image (with excluded contribution of the spatial frequencies outside of the chosen range), should be obtained by the inverse Fourier transformation of the matrix **G**″.

To illustrate the results of suggested data processing, i.e., elimination of the high spatial frequencies and zero-frequency components present in the raw signal, a modified image of the same region of interest, as in Fig. 1(b), is presented in Fig. 3. Chosen values of $k=1$ and $K=100$ [see Eq. (2)] correspond to spatial frequencies of ~20 and ~0.2 mm^{-1}, respectively [estimated, as $1/2\pi k(0.0075)$]. Thus, the data processing removes image irregularities less than 0.05 and greater than 5 mm. To make a reasonable choice of k and K indices in this case, a subjective perception of the image structure of Fig. 3 was accepted. Despite the loss of some information, this procedure made visible structural characteristics that were previously masked by the high-spatial-frequency noise in the original image [compare Figs. 1(b) and 3]. Intensity noise can originate either from speckles or skin surface roughness, which may give some specular reflection in the direction of the camera lens. Additional noise in the polarization degree
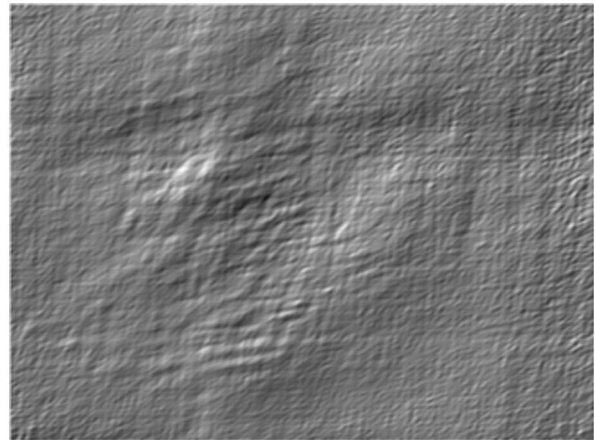

Fig. 3 Image of DP of the region presented in Fig. 2 after data processing involving Fourier transformations and filtering, as described in the text.

image may be caused by a reorientation of polarized light due to light scattering or effects of randomly oriented birefringent tissue fibers. Besides, amplitude of noise, presented in matrix **G**, should be at least doubled, in accordance with Eq. (1).

4 Pearson Correlation Analysis

It is worth estimating the size and orientation of heterogeneities that stand out from the noise in Fig. 1(b), but still are noticeably distorted by it. To do this, we developed a fractional statistical analysis of the digital pattern, based on calculating the Pearson correlation coefficient. To evaluate spatial correlation in the raw data, we introduce two similar submatrices **A** and **B** of size $(2m+1) \times (2n+1)$ that are formed from the original matrix **G**. Matrix **A** is centered at a given point with coordinates (indices) (i_0, j_0), while matrix **B** is shifted relative to **A** by some vector **r**. The Pearson correlation coefficient between two matrices **A** and **B** is defined by the expression

$$\text{corr}\,(\mathbf{A}, \mathbf{B}) = \frac{\sum_{k=0}^{m} \sum_{l=0}^{n} (A_{k,l} - \bar{A})(B_{k,l} - \bar{B})}{mn\,\text{stdev}\,\mathbf{A}\,\text{stdev}\,\mathbf{B}}, \quad (3)$$

where $\bar{A}$ and $\bar{B}$ are the mean values of the elements of matrices **A** and **B**, and stdev (**A**) and stdev (**B**) are the standard deviations of elements in matrices **A** and **B**, respectively. The coefficient corr (**A**, **B**) can vary between 1 and −1, depending on the degree of correlation between **A** and **B**; correlation is maximal for corr (**A**, **B**)=1 or −1 and minimal for corr (**A**, **B**)=0. The minus sign of the correlation coefficient means that the corresponding elements have opposite signs relative to the mean values. To reveal possible structural similarities between various regions of the image (pattern), matrix **A** should be fixed at some reference point, while matrix **B** is scanned throughout the image, providing the correlation coefficient, as a function of **r**. Such an approach is very simple and easy to implement. However, up to now the Pearson correlation was not generally used for enhancement of specific pattern features or their recognition. Instead, various Fourier, wavelet, and correlation functional analyses have been used to characterize structural features of various patterns[20] and specific features of polarization patterns of biological tissues.[21] We propose here the Pearson analysis as an alternative simple method.

Evidently, the easiest analysis may be performed by scanning matrix **B** throughout pattern over all integer values along x and y axes. To estimate the dependence of the Pearson correlation coefficient on the arbitrary scale and azimuthal angle, we superimpose an auxiliary submatrix **SM** rotated at this angle, which includes the region of interest, onto the original matrix **G**. Values of the nearest pixels of the original matrix **G** are attributed to the corresponding pixel values of submatrix **SM**. Figure 4 geometrically demonstrates this procedure. To create submatrix **SM** of size $(2m+l) \times (2n+1)$, centered at a point with coordinates (indices) (i_0, j_0) and rotated at an angle α relative to the direction of the rows of the matrix **G**, we used the following shift and rotation transformations:
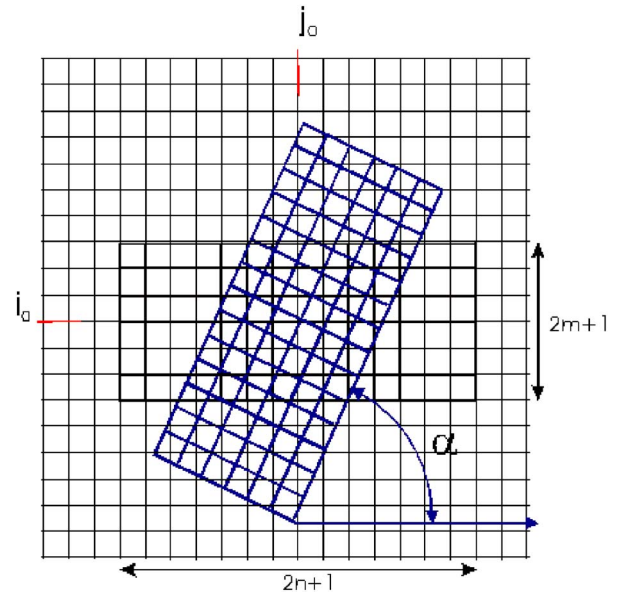

Fig. 4 Illustration of the procedure to design the submatrix of size $(2n+1) \times (2m+1)$, centered at an arbitrary point (j_0, i_0) of original matrix and tilted at an angle α with respect to the rows of original matrix (x axis).

$$\begin{bmatrix} i \\ j \end{bmatrix} = \begin{bmatrix} \cos(\alpha) & -\sin(\alpha) \\ \sin(\alpha) & \cos(\alpha) \end{bmatrix} \begin{bmatrix} p - n - i_0 \\ q - m - j_0 \end{bmatrix} + \begin{bmatrix} i_0 \\ j_0 \end{bmatrix}, \quad (4)$$

where index $p = 0, 1, \ldots, 2n$, index $q = 0, 1, \ldots, 2m$. The relationship between the appropriate pixel values of the original matrix **G** and the newly designed submatrix **SM** is given by

$$SM_{p,q}(i_0, j_0, \alpha) = G_{i', j'}. \quad (5)$$

Here i' and j' are rounded to integer values of i and j, respectively. Once a submatrix **SM** is created, a straightforward procedure is to analyze the behavior of the Pearson correlation coefficient for a given azimuth angle α, as a function of scale by shifting submatrix **B** at different integer values with respect to submatrix **A**, implying that both **A** and **B** are **SM** submatrices of the same dimensions. Matrix **A** is centered in the region of interest [point (i_0, j_0) of matrix **G**].

Figure 5 shows the behavior of the Pearson correlation coefficient in the vicinity of point A [shown in Fig. 1(b)], close to the center of the irradiated skin region, for two perpendicular directions that were tilted relative to the horizontal axis at angles of 10 and 100 deg, respectively. The presented data were calculated for submatrices of 29×31 pixels that correspond to a size of 0.22×0.23 mm as the region of interest. Figure 5 shows that for 10 deg, the correlation coefficient drops to a level of about 0.6 and then remains almost constant up to a distance of about 0.5 mm; for 100 degs there is an obvious periodicity with spatial period of approximately 0.26 mm. This periodicity may be explained by the existence of some elongated structure in the vicinity of this point. The azimuthal dependence of the Pearson correlation coefficient presented in Fig. 6 not only supports this conclusion, but also helps to determine the directionality of this structure. In fact, the azimuth variation of the Pearson coefficient may be realized by scanning over a circumference of a given radius. It
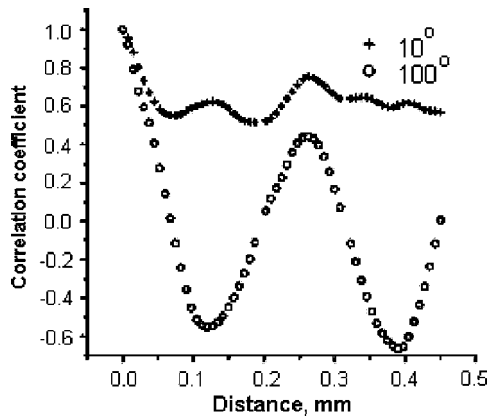
Fig. 5 Pearson correlation coefficient in the vicinity of point *A* of Fig. 1(b), as a function of distance for azimuthal angles 10 and 100 deg.

Fig. 7 Pearson correlation coefficient in the vicinity of point *B* of Fig. 1(b), as a function of distance for azimuthal angles −10 and 80 deg.

may provide additional information regarding the structural characteristics in the vicinity of the point of interest.

Our quantitative analysis shows that the spatial correlation coefficient behaves differently, as a function of scale, far from the x-ray-irradiation zone [undamaged skin, e.g., close to point *B* in Fig. 1(b)]. As presented in Fig. 7, the correlation coefficient decreases with increasing distance, reaching almost zero at distances greater than 0.05 mm. This behavior demonstrates a low (practically nonexistent) level of any regular structure at the scales shown for both azimuths. Angular dependence of the correlation function, centered at point *B*, can substantiate this conclusion.

The described imaging technique has a potential use for estimating characteristic size and directionality of superficial hidden structures, for example, in dermatology or stomatology. How deeply a hidden structure may be traced by this analysis strongly depends on the scattering coefficient of the tissue and on the birefringence of superficial tissue layers. Polarized photons lose their initial polarization state in about 5 to 10 scattering events. Thus, residual degree of polarization remains detectable for photon path lengths of a few millimeters in tissues.[22] The scattering coefficient of the human derma
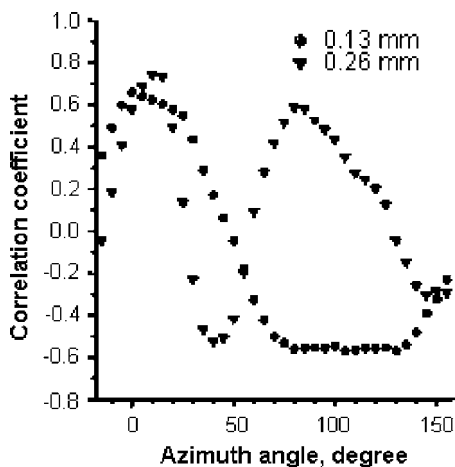
is about 200 cm^{-1} in the visible range.[23] Correspondingly, tissue structures at depths of 250 to 500 μm below the skin surface are expected to be accessible for polarization analysis. When fibrosis has developed, the derma becomes thinner. This fact opens a promising opportunity to discover the early stage of fibrosis. Note that the probe light with wavelengths longer than the one used here (630 nm) can penetrate deeper into the tissue, since scattering coefficient decreases with wavelength.

5 Conclusions

Measurements of the DP enable digital polarized photography to reveal hidden structures beneath the skin surface, when the skin is characterized by special conditions such as fibrosis from x-ray irradiation. The Fourier transformation of DP data with subsequent elimination of high spatial frequencies, followed by inverse Fourier transformation, substantially enhances the informational content of the obtained images. Such a methodology makes it possible to estimate the characteristic sizes and directionality of possible regular structures. In this way, Pearson correlation analysis enables us to better investigate internal skin structures.

References

1. I. M. Stockford, S. P. Morgan, P. C. Chang, and J. G. Walker, "Analysis of the spatial distribution of polarized light backscattered from layered scattering media," *J. Biomed. Opt.* **7**, 313–320 (2002).
2. S. L. Jacques, J. R. Roman, and K. Lee, "Imaging superficial tissues with polarized light," *Lasers Surg. Med.* **26**, 119–129 (2000).
3. R. R. Anderson, "Polarized light examination and photography of the skin," *Arch. Dermatol.* **127**, 1000–1005 (1991).
4. A. N. Yaroslavsky, V. Neel, and R. R. Anderson, "Demarcation of nonmelanoma skin cancer margins in thick excisions using multispectral polarized light imaging," *J. Invest. Dermatol.* **121**, 259–266 (2003).
5. S. L. Jacques, J. C. Ramella-Roman, and K. Lee, "Imaging skin pathology with polarized light," *J. Biomed. Opt.* **7**, 329–340 (2002).
6. J. C. Ramella-Roman, K. Lee, S. A. Prahl, and S. L. Jacques, "Design, testing, and clinical studies of a handheld polarized light camera," *J. Biomed. Opt.* **9**, 1305–1310 (2004).

Fig. 6 Pearson correlation coefficient in the vicinity of point *A* of Fig. 1(b), as a function of azimuthal angles for two distances 0.13 and 0.26 mm.
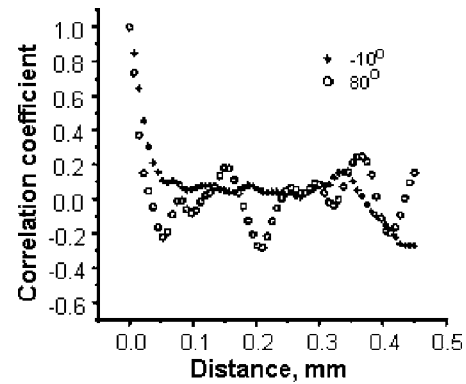
7. D. A. Zimnyakov, Y. P. Sinichkin, I. V. Kiseleva, and D. N. Agafonov, "Effect of absorption of multiply scattering media on the degree of residual polarization of backscattered light," *Opt. Spectrosc.* **92**, 765–771 (2002).

8. M. Mujat, "Measurement of structure-induced polarization features in forward scattering from collections of cylindrical fibers," *J. Quant. Spectrosc. Radiat. Transf.* **70**, 555–567 (2001).

9. F. Berthod, L. Germain, H. Li, W. Xu, O. Damour, and F. A. Auger, "Collagen fibril network and elastic system remodeling in a reconstructed skin transplanted on nude mice," *Matrix Biol.* **20**, 463–473 (2001).

10. J. W. Hopewell, "The skin: its structure and response to ionizing radiation," *Int. J. Radiat. Biol.* **57**, 751–773 (1990).

11. K. C. Flanders, C. D. Sullivan, M. Fujii, A. Sowers, M. A. Anzano, A. Arabshahi, C. Major, C. Deng, A. Russo, J. B. Mitchell, and A. B. Roberts, "Mice lacking Smad3 are protected against cutaneous injury induced by ionizing radiation," *Am. J. Pathol.* **160**, 1057–1068 (2002).

12. T. J. Franklin, "Current approaches to the therapy of fibrotic diseases," *Biochem. Pharmacol.* **49**, 267–273 (1995).

13. T. J. Franklin, "Opportunities for the discovery of novel therapies for fibrotic diseases," *Exp. Nephrol.* **3**, 143–147 (1995).

14. H. M. Kagan, "Intra- and extracellular enzymes of collagen biosynthesis as biological and chemical targets in the control of fibrosis," *Acta Trop.* **77**, 147–152 (2000).

15. J. Rogowska and M. E. Brezinski, "Image processing techniques for noise removal, enhancement and segmentation of cartilage OCT images," *Phys. Med. Biol.* **47**, 641–655 (2002).

16. R. el Nabout, M. Martin, J. Remy, P. Kern, L. Robert, and C. Lafuma, "Collagen synthesis and deposition in cultured fibroblasts subcutaneous radiation induced fibrosis modification as a function of cell aging," *Matrix* **9**, 411–420 (1989).

17. C. Brosseau, *Fundamentals of Polarized Light: A Statistical Optics Approach*, Wiley, New York (1998).

18. A. P. Sviridov, D. A. Zimnyakov, Y. P. Sinichkin, L. N. Butvina, A. J. Omelchenko, G. S. Shakh, and V. N. Bagratashvili, "Attenuated total reflection Fourier transform infrared and polarization spectroscopy of in vivo human skin ablated, layer by layer, by erbium:YAG laser," *J. Biomed. Opt.* **9**, 820–827 (2004).

19. O. Korotkova and E. Wolf, "Changes in the state of plarfization degree of a random electromagnetic beam on propagation," *Opt. Commun.* **246**, 35–43 (2005).

20. F. T. S. Yu and J. Suganda, "Optical pattern recognition," *Cambridge* 440 (1998).

21. O. V. Angelsky, G. V. Demianovsky, A. G. Ushenko, D. N. Burkovets, and Y. A. Ushenko, "Wavelet analysis of two-dimensional birefringence images of architectonics in biotissues for diagnosing pathological changes," *J. Biomed. Opt.* **9**, 679–690 (2004).

22. V. Sankaran, J. T. Walsh Jr., and D. J. Maitland, "Comparative study of polarized light propagation in biological tissues," *J. Biomed. Opt.* **7**, 300–306 (2002).

23. W. -F. Cheong, S. A. Prahl, and A. J. Welch, "A review of the optical properties of biological tissues," *IEEE J. Quantum Electron.* **QE-26**, 2166–2185 (1990).